Electronic Supplementary Material (ESI) for Journal of Materials Chemistry C.

Supporting Information

Design of Thermally Activated Delayed Fluorescence Emitters for Organic Solid-State Microlasers

Shuai Li,[§,a] *Xue Jin,*[§,b] *Zhenyi Yu,*[*,b] *Xiaoxiao Xiao,*[c] *Hua Geng,*[c] *Qing Liao,*[c] *Yi Liao,*[c]
Yishi Wu,[c] *Wenping Hu*[b] *and Hongbing Fu* [*,a,c]

[a] Institute of Molecule Plus, Tianjin University, and Collaborative Innovation Center of Chemical Science and Engineering (Tianjin), Tianjin 300072, P. R. China

[b] Tianjin Key Laboratory of Molecule Optoelectronic Sciences, Department of Chemistry, School of Sciences, Tianjin University, Tianjin 300072, P. R. China
E-mail:

[c] Beijing Key Laboratory for Optical Materials and Photonic Devices, Department of Chemistry, Beijing Advanced Innovation Center for Imaging Technology, Capital Normal University, Beijing 100048, P. R. China

* E-mail: hbfu@cnu.edu.cn; zhenyi.yu@tju.edu.cn

§ S.L. and X.J. contributed equally.

Contents

1. Note S1. General Information
2. Note S2. Synthesis and Characterization
3. Note S3. Spectral characterization and photophysical parameters
4. Note S4. X-Ray crystallography
5. Note S5. Theoretical calculation methods
6. Note S6. Solvatochromic effect
7. Additional data and results
8. References

Note S1. General Information

All the chemicals and reagents were purchased from commercial sources and used as received without further purification. All reactions involving air-sensitive reagents or intermediates were carried out under argon atmosphere. If not indicated otherwise, all photophysical measurements were performed in dried solvents. The molecule synthesized was purified by column chromatography and recrystallization from dichloromethane and hexane for two times, and fully characterized by ^{1}H NMR, ^{13}C NMR and high resolution mass spectroscopies (HRMS).

^{1}H NMR (400 MHz) and ^{13}C NMR (151 MHz) spectra were recorded in deuterated solvents on a Bruker ADVANCE 400 NMR Spectrometer. Tetramethylsilane (TMS) was used as the internal standard. HRMS were recorded on a GCT premier CAB048 mass spectrometer operating in MALDI-TOF mode.

Note S2. Synthesis and Characterization

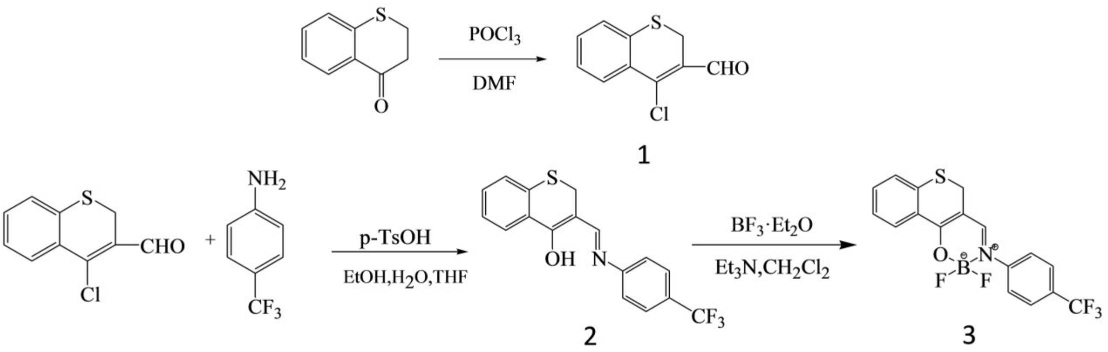

Scheme S1. The synthetic routes of *(E)-3-(((4-Trifluoromethyl)imino)methyl)-2H -thiochroman -4-olate•*BF_2 (SBF$_2$BTF)

2.1 Synthesis of 4-chloro-2H-thiochromene-3-carbaldehyde (1) [1]

The reaction is obtained by the Vilsmeier-Haack-Arnold Reaction (VHA) reaction. 10 ml of DMF was added to an anhydrous Schlenk reaction tube and anaerobically operated through a double row of tubes. 18.2 mmol $POCl_3$ (1.7 mL, 1.2 eq.) was added dropwise to ice-cold anhydrous DMF, then 15.2 mmol thiochroman-4-one (1.6 mL, 1 eq.) was added dropwise. The reaction mixture was stirred in an ice bath for 30 minutes and then heated to 80° C. and stirred for 2 hours. After the reaction was complete, it was quenched with 6 mL of ice-cold aqueous sodium acetate solution (25%). The crude sample was extracted twice with diethyl ether, and the organic layers were combined, washed with saturated brine, dried over sodium sulfate, and concentrated to give compound 4-chloro-2H-thiobenzopyran-3-carbaldehyde (brown oily liquid). Yield 86%. The resulting product can be used in the next stage without further purification.

2.2 Synthesis of (E)-3-((4-(trifluoromethyl)phenylimino)methyl)-2H-thiochromen -4-ol (2)

3.0 mmol of 4-chloro-2H-thiobenzopyran-3-carbaldehyde (0.632 g) and 3.0 mmol of 4-(trifluoromethyl)benzenamine (0.483g) were dissolved in ethanol (15mL), tetrahydrofuran (THF) (15 mL) and water (6 mL) in a mixture. After adding 1.0 mmol of p-toluenesulfonic acid (p-TsOH) (0.516 g), the reaction mixture was stirred at 80°C for 3 h. After the reaction was completed, the product was concentrated to a solid. The resulting product can be used in the next stage without further purification.

2.3 Synthesis of (E)-3-(((4-Trifluoromethyl)imino)methyl) -2H-thiochroman -4-olate•BF_2 (3)

(E)-2-(((4-nitrophenyl)imino)methyl)-3,4-dihydronaphthalen-1-ol (1.0 mmol) was dissolved in CH_2Cl_2 containing Et_3N (2.0 mL, 14.4 mmol) at 0-5°C. $BF_3 \cdot Et_2O$ (≥46.5 % BF_3 basis, 3.0 mL) was slowly added. The reaction mixture was stirred at room temperature for 1 hour, after the reaction was completed (monitored by TLC). Then quenched by adding 20% sodium bicarbonate solution (10-20 mL) until PH=7. The separated organic layer was dried over anhydrous Na_2SO_4 and evaporated in vacuum. Petroleum ether and ethyl acetate = 10:1-7:1 were selected as developing agent for column chromatography. The yellow solid powder SBF_2BTF was obtained. The total yield in two steps is 38%.

(E)-3-(((4-Trifluoromethyl)imino)methyl) -2H-thiochroman -4-olate•BF_2. Yellow solid powder. Yield: 50% . ^1H NMR (300 MHz, CD_2Cl_2) δ 8.04 (d, J = 8.0 Hz, 1H), 7.88 (s, 1H), 7.70 (d, J = 8.6 Hz, 2H), 7.56 (d, J = 8.2 Hz, 2H), 7.33 (m, 3H), 3.78 (s, 2H). ^{13}C NMR (151 MHz, $CDCl_3$ 300 K): δ169.83, 159.48, 145.73, 140.44, 134.00, 130.34, 130.12, 129.36, 128.81, 128.14, 127.17, 126.64, 125.18, 124.02, 123.37, 101.98, 27.17. HRMS (MALDI-TOF, *m/z*):calcd for $C_{17}H_{11}BF_5NOS$, 383.0575. Found, 383.0525.

Note S3. Spectral Characterization and Photophysical Parameters

3.1 Steady-State Spectroscpic Measurements.

The UV-visible absorption spectra were measured on a Shimadzu UV-3600 spectrometer with a slit width of 1 nm. The fluorescence emission spectroscopy and absolute luminescence quantum yield were measured on a Hitachi F-4600 spectrophotometers equipped with a xenon arc lamp and an integrating sphere.

3.2 The lifetime, time-resolved emission spectra Measurement.

We built the picosecond time resolution device independently for testing, the device configuration is as follows: the second harmonic (400 nm, 150 fs, 1 kHz) of a regenerative amplifier (Spitfire, Spectra Physics) seeded with a mode-locked Ti:sapphire laser (Tsunami, Spectra Physics) was used to excite the samples (liquid sample in a 10 mm cuvette) at the front surface with an incidence angle of 45°. In order to avoid interference as much as possible, the excitation pulse light and the signal light are spatially perpendicular to each other. The signal collected along the direction normal to the sample surface was dispersed by a polychromator (250is, Chromex) and detected with a streak camera (C5068, Hamamatsu Photonics). The spectral resolution was 0.2 nm, and the temporal resolution was slightly different depending on the delay width used. Dissolved oxygen was removed by bubbling in the solution with high purity nitrogen for 30 minutes.

3.3 Measurement of singlet oxygen yield.

Through continuous photolysis procedure, the quantum yield for generation of singlet oxygen has been described as below. Briefly, 9,10-diphenylanthracene (DPA) was used as a substrate to intercept singlet oxygen because of its nonradiative deactivation. The consumption of singlet oxygen in air-saturated CH_2Cl_2 solution was measured under 444 nm continuous laser irradiation. The concentration of DPA was prepared at $\sim 8 \times 10^{-4}$ M. To ensure that an equal number of photons were absorbed at the same irradiation time in all experiments, the absorption of each photosensitizer was adjusted to 0.50 in a 1 cm cell at the wavelength of 375 nm. Therefore, the DPA can efficiently intercept the singlet oxygen. hypocrellin A (HA) (Φ_Δ= 0.84 in CH_2Cl_2) was used as the reference. [2] The singlet oxygen quantum yield was calculated using the equation on:

$$\Phi_\Delta^S = \Phi_\Delta^R \times \frac{k^S / A^S}{k^R / A^R}$$

The *k* is the slope of singlet oxygen consumption, the A is the absorbance at 375 nm and the suffixes “S” and “R” refer to the sample and the reference, respectively.

Note S4. X-Ray Crystallography

The single crystal sample of SBF_2BTF was achieved from slowly evaporative crystallization using ethanol/dichloromethane mixture (3:1, v/v). Single crystal data was collected on a SuperNova, Dual, AtlasS2 diffractometer using graphite monochromated CuKα radiation (λ = 1.54178 Å). The crystal was kept at 100.00 (10) K during data collection. Using Olex2, the structure was solved with the ShelXT structure solution program using Intrinsic Phasing and refined with the ShelXL refinement package using Least Squares minimization.

Crystal data for SBF_2BTF (CCDC-1914187): $C_{17}H_{11}BF_5NOS$, *MW*=383.14, monoclinic, $P2_1/c$, a = 8.2610 (5) Å, b = 12.9941 (3) Å, c = 31.0168 (9) Å, $\alpha = \gamma =$ 90°, β = 93.377(4)°, V = 3323.6(9)$Å^3$, Z=8, *D*c = 1.587 g cm^{-3}, μ = 0.259 mm^{-1}, *F*(000) = 698, *T* = 173(2)K, 2*θ*max =25.247 (99.6%), 3380 independent reflections (*R*int =0.0427), Goodness-of-fit on F^2= 1.159, *R*1 = 0.0579, w*R*2 = 0.1105 (all data).

Note S5. Theoretical calculation methods

Geometrical and electronic structures of all states were calculates by Gaussian 09 program package. [3] The equilibrium geometries of ground (S_n) and triplet states (T_n) in DCM solution were determined at B3LYP/6-31G* level using density functional theory (DFT) and time-dependent DFT (TDDFT) combined with polarizable continuum model (PCM). Based on this method, the nature transition orbitals (NTOs) were also calculated for S_1 and T_n states. Common pure organic small molecules and molecules with charge transfer features can be sufficiently described by the above method. At the same level, the spin-orbit coupling (SOC) matrix elements between singlet and triplet states are given by PySOC program. [4] And the CT content was calculated quantitatively through the MULTIWFN program.[5]

Note S6. Solvatochromic effect

The influence of solvent environment on the optical property of our compound can be understood using the Lippert-Mataga equation:[6]

$$hc\,(\nu_a - \nu_f) = hc\,(\nu_a^0 - \nu_f^0) + \frac{2\Delta\mu^2}{a^3} f(\varepsilon, n), \quad a = \sqrt[3]{\frac{3M}{4\pi d N_a}}$$

where f is the orientational polarizability of the solvent, $\nu_a - \nu_f$ is the Stokes shift, h is Planck's constant, c is the velocity of light, $\Delta\mu = \mu_e - \mu_g$ is the difference in the dipole moment of fluorophore between the excited (μ_e) and the ground (μ_g) states, a is the solvent cavity (Onsager) radius, derived from the Avogadro's number (N_a), molecular weight (M), and density (d=1.0 g/cm^3); ε and n are the solvent dielectric and the solvent refractive index, respectively; $f(\varepsilon, n)$ can be calculated respectively as follows:

$$f(\varepsilon, n) = \frac{\varepsilon - 1}{2\varepsilon + 1} - \frac{n^2 - 1}{2n^2 + 1}$$

Therefore, based on equation, the change in dipole moment, $\Delta\mu = \mu_e - \mu_g$, can simply be estimated from the slope of a plot of ν_a-ν_f against Δf.

Additional data and results

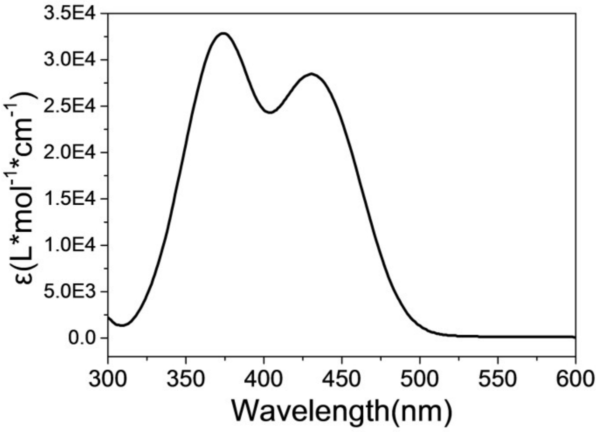

Fig. S1. Electronic absorption spectra of compound SBF_2BTF in DCM.

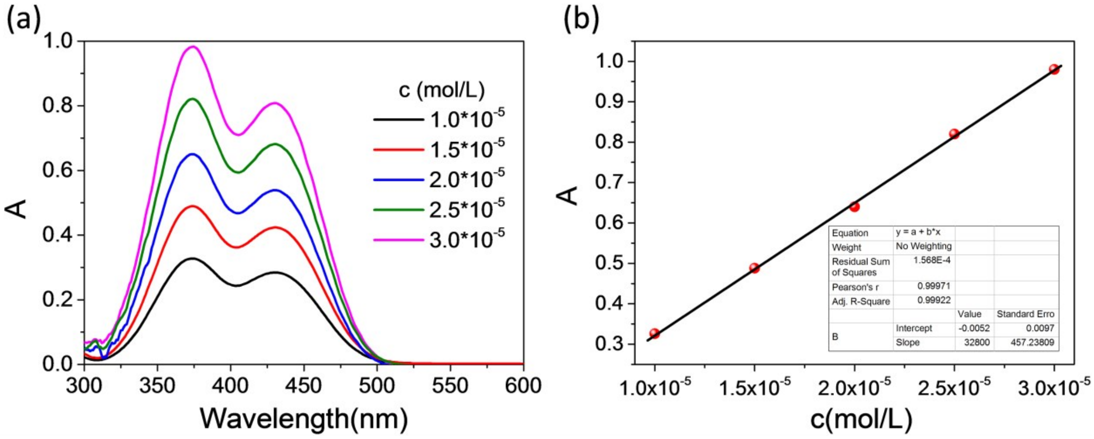

Equation	y = a + b*x		
Weight	No Weighting		
Residual Sum of Squares	1.568E-4		
Pearson's r	0.99971		
Adj. R-Square	0.99922		
		Value	Standard Erro
B	Intercept	-0.0052	0.0097
	Slope	32800	457.23809

Fig. S2. Concentration dependence of the absorbance of SBF_2BTF in DCM at 374 nm.

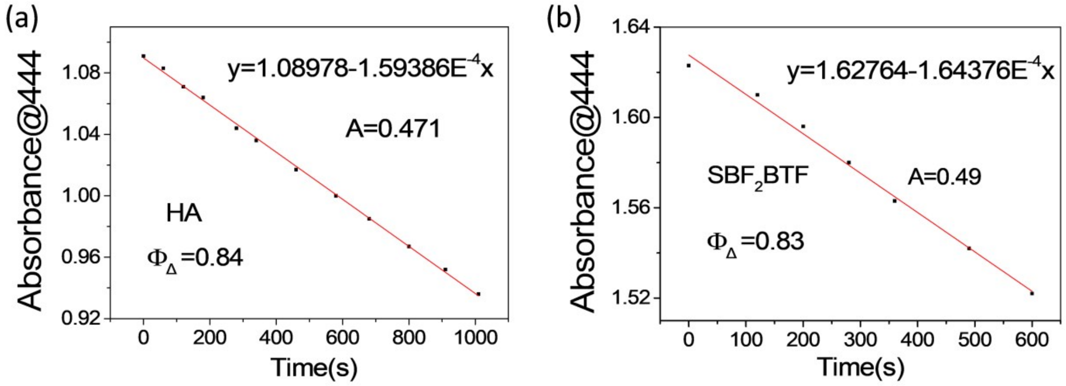

Fig. S3. The decrease of the absorbance at 444 nm of DPA as a function of irradiation time for (a) hypocrellin A, (b) for compound SBF$_2$BTF. The linear fitting results are also shown.

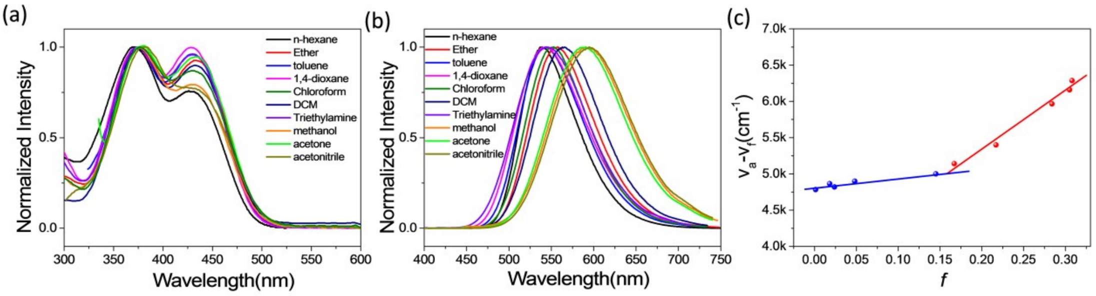

Fig. S4. The UV-visible spectra (a) and PL spectra (b) of SBF$_2$BTF, measured in different solvents with increasing polarity (the orientational polarizability of solvent, *f* – hexane: 0.0012; toluene: 0.014; 1,4-dioxane: 0.0237; triethylamine: 0.048; trichloromethane: 0.154; ether: 0.167; dichloromethane: 0.217; acetone: 0.284; acetonitrile: 0.305 and methanol: 0.308). (c) Linear correlation of orientation polarization (*f*) of solvent media with the Stokes shift (v_a–v_f) for SBF$_2$BTF.

The difference between the dipole-moments (Δμ) of SBF$_2$BTF in the lowest excited S$_1$ state (μ_e) and in the ground S$_0$ state (μ_g) was estimated from the slope of a plot of Stokes shift (v_a–v_f) versus the solvent polarity. The (μ_g) is calculated as 6.47 D through Gaussian 09 program package at the B3LYP/6-31G* level. Through the analysis of the fitted line in low polarity solvents, its corresponding μ_e was calculated to be 7.87 D, in the high-polarity solvents the μ_e was calculated to 14.37 D.

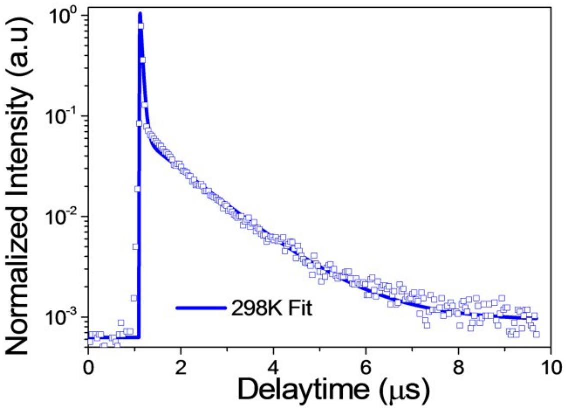

Fig. S5. The PL decay of SBF_2BTF in DCM at RT (blue line).

Table S1. Photophysical parameters of SBF_2BTF compound in CH_2Cl_2 solution.

Compound	k_r [s^{-1}]	Φ_p [%]	Φ_d [%]	Φ_{ISC} [%]	ΔE_{ST} [eV]
SBF_2BTF	4.4×10^7	3.6	8.4	83	0.12

Abbreviations: k_r, radiative rate constant ($S_1 \rightarrow S_0$), $k_r = \Phi_p / \tau_r$; Φ_p, quantum efficiency for prompt fluorescence component; Φd, quantum efficiency for delayed fluorescence component; Φ_{ISC}, intersystem-crossing quantum efficiency; ΔE_{ST}, energy gap between $S_1$and T_2, $\Delta E_{ST} = -RT \ln (3\, k_d / k_r)$, $k_d = \Phi_d / (\Phi_{ISC} \tau_d)$.

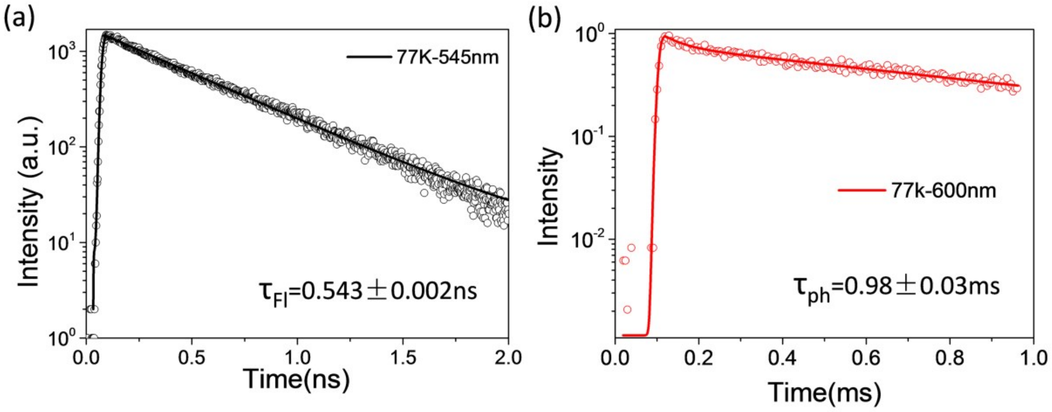

Fig. S6. Fluorescence (a) and phosphorescence (b) PL decay curves at 77K.

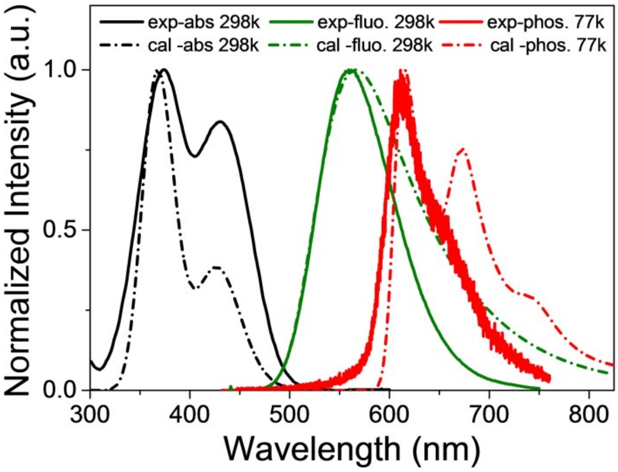

Fig. S7. Steady-state absorption (black line), fluorescence spectrum (green line) at room temperature and the phosphorescence spectrum (red line) at 77K in DCM solutions. The calculated theoretical absorption, fluorescence and phosphorescence spectra are shown as corresponding dashed lines.

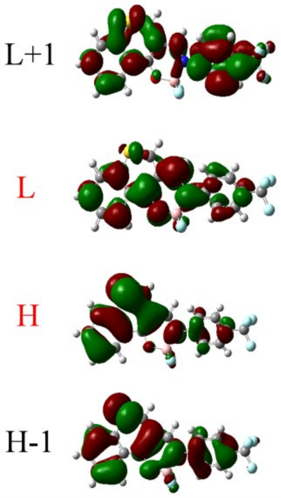

	Transition (%)	
S_1	H-1→L	5.35
	H→L	93.86
T_2	H-1→L	62.39
	H→L	31.48
	H→L+1	2.18
T_1	H-1→L	31.88
	H→L	64.04

Fig. S8. Electronic transition characters, and involved frontier molecular orbitals.

Table S2. The reorganization energies during the different decay processes for SBF_2BTF.

	$S_1 \rightarrow S_0$	$T_1 \rightarrow S_0$	$S_1 \rightarrow T_1$	$S_1 \rightarrow T_2$	$T_2 \rightarrow T_1$
cm^{-1}	1970.35	2183.98	641.98	694.01	1443.52
meV	244	271	80	86	179

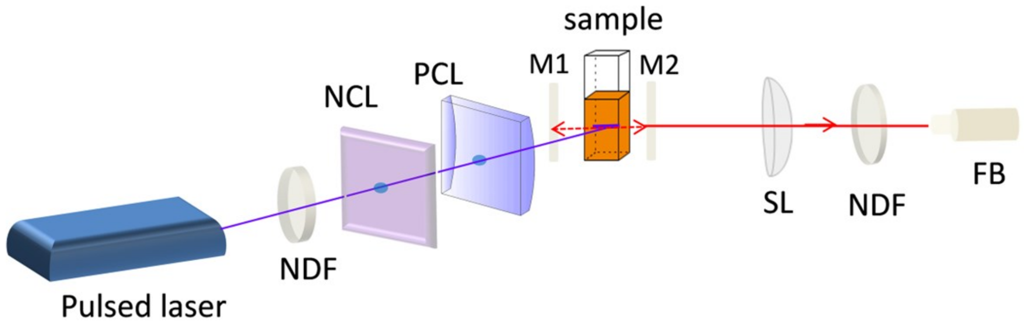

Scheme S3. Set-up for laser studies. NDF: neutral density filters; NCL: negative cylindrical lens; PCL: positive cylindrical lens; M_1, M_2: silver mirrors with 90% reflectivity and 50% reflectivity; SL: spherical lens; FB: fibre bundle.

Scheme S3 shows a sketch of an experimental setup used for the solution sample stimulated emission experiments. The sample was optically pumped at 400 nm excitation laser using a femtosecond excitation laser pulsed at 150 fs, 1 kHz. The pump energy was controlled through calibrated neutral-density filters. The femtosecond excitation laser was focused by a cylindrical lens (with focal length f = 20 cm) to a stripe into a rectangle strip (0.018 cm width and variable length) on the surface of sample. The oscillating chamber (1.5 cm length) consists of two silver mirrors with 90% reflectivity and 50% reflectivity. The stimulated emission was collected with a 15 cm focal length spherical lens, focused onto a fiber bundle and detected with a spectrograph （Spectropro-550i, Acton Research Corp）equipped with a thermoelectrically cooled charge-coupled detector (CCD) （SpectruMM：GS 128B） and a photomultiplier for the photo stability measurements. Calibrated neutral-density filters were used before the fiber bundle to avoid saturation of the detector.

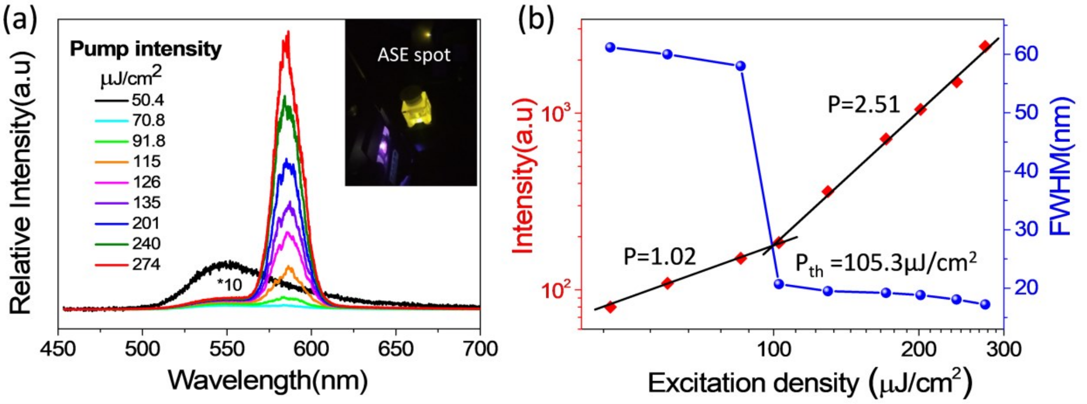

Fig. S9. (a) PL spectra of dye lasers based on SBF$_2$BTF in DCM solution collected under different excitation intensities below and above the lasing threshold. Inset: Photographs of dye laser under operation. (b) The output intensity of the dye lasers and the FWHM of the emission peak as a function of the pump density.

Excitingly, we observed good stimulated emission of SBF$_2$BTF molecules in DCM solution. Solution of SBF$_2$BTF:DCM (6 mM) was transversely excited by the pulses of femtosecond excitation laser (Scheme S3). Fig. S9 shows the emission spectrum of SBF$_2$BTF in DCM solution below and above the ASE threshold. At low pumping density, the PL spectra exhibit broad peaks of spontaneous TADF emission (black line). When the pumping density is increased above the threshold, a sharp peak emerge centered at 584 nm. And the full width at half maximum (FWHM) decreases from 60 nm below the threshold to 18 nm above the threshold (blue line of Fig. S9b). This collapse of the emission spectrum is one of the signatures of the presence of stimulated emission. We also plot the integrated PL intensities as a function of the pump density in the Fig. S9b. An abrupt change in the slope is clearly observed and this can be interpreted as an laser threshold at P_{th} = 105.3 μJ/cm^2. Note that when the femtosecond laser pumping density increases well above the laser threshold, the SBF$_2$BTF in DCM solution exhibits a strong yellow ASE light spot (inset image of Fig. S9a).

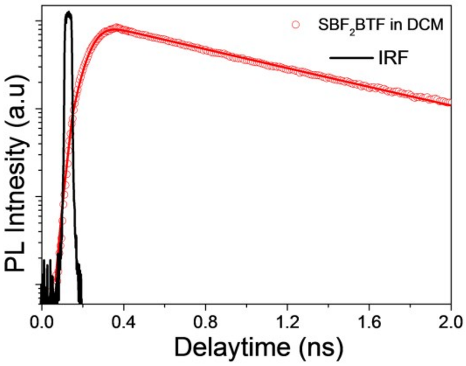

Fig. S10. PL decay of prompt components of SBF_2BTF in degassed DCM.

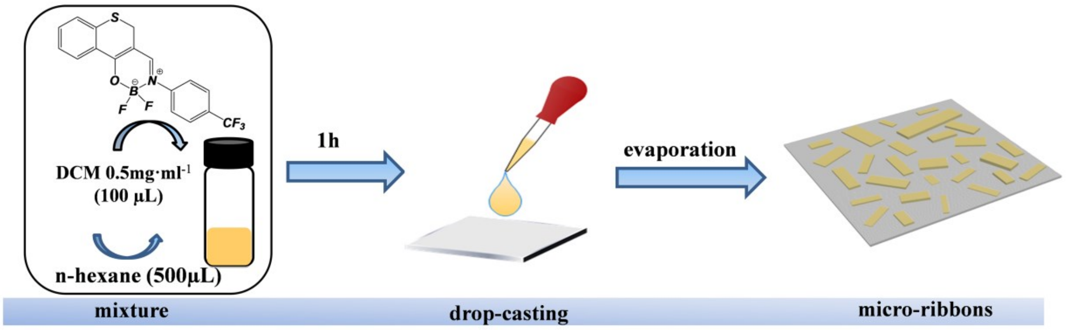

Fig. S11. The scheme of preparing of the SBF_2BTF microribbons (MRs).

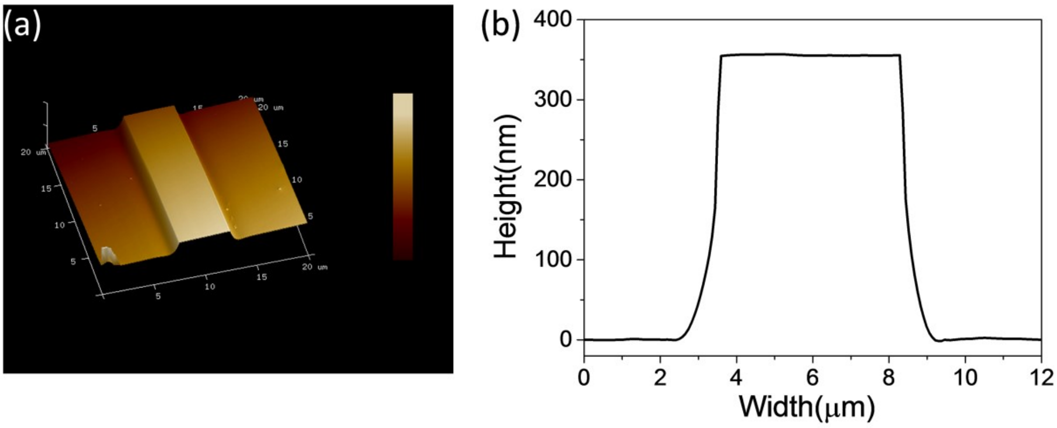

Fig. S12. (a) AFM image of a single microribbon. (b) The corresponding height profiles.

Table S3. Photophysical parameters of SBF_2BTF monomers in the DCM and solid-state MRs.

SBF_2BTF	λ_{abs} [nm]	λ_{Pl} [nm]	τ [μs]	$\Phi_{pl}{}^{a}$ [%]	$\lambda_{Fluo}{}^{b}$ (nm)	$\lambda_{Phos}{}^{b}$ (nm)	$\tau_F{}^{b}$ [ns]	$\tau_{Phos}{}^{b}$ [ms]
monomer	374,430	560	0.89	12	545	612	0.54	0.98
MRs	366,444	556	0.31	6.5	550	610,650	0.65	0.16,0.24

[a] Absolute photoluminescence quantum yield. [b] Measured at 77 K using a streak camera.

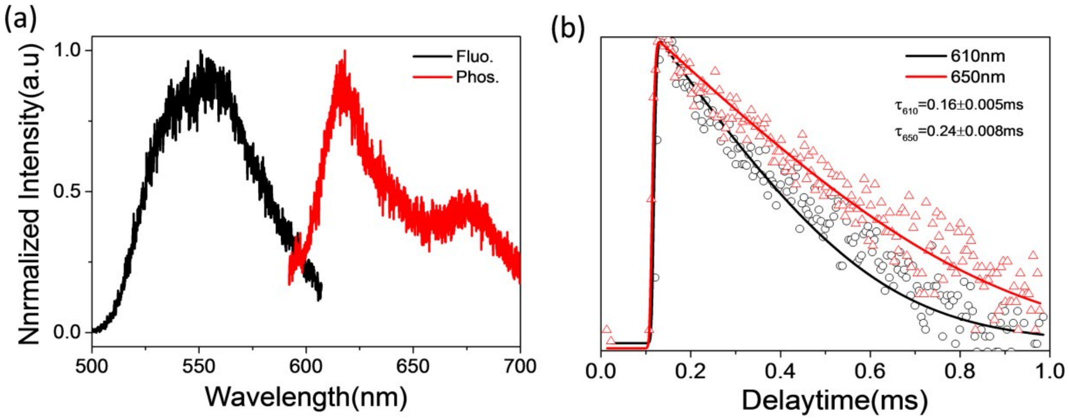

Fig. S13. (a) fluorescence (t=10 ns) and phosphorescence (t=1ms) PL spectra of microribbons at 77K. (b) PL decay curves of microribbons measured for persistent emission and for fast emission (insert) at 77K.

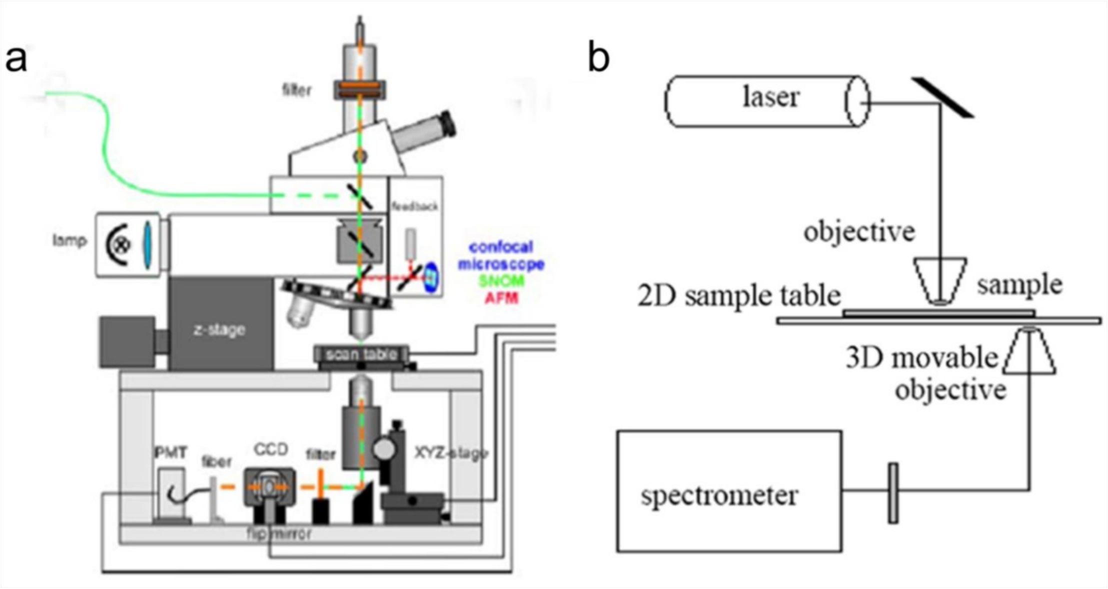

Fig. S14. Schematic illustration of (**a**) the near-field scanning optical microscopy and (**b**) the transmittance optical path for the waveguide measurements.

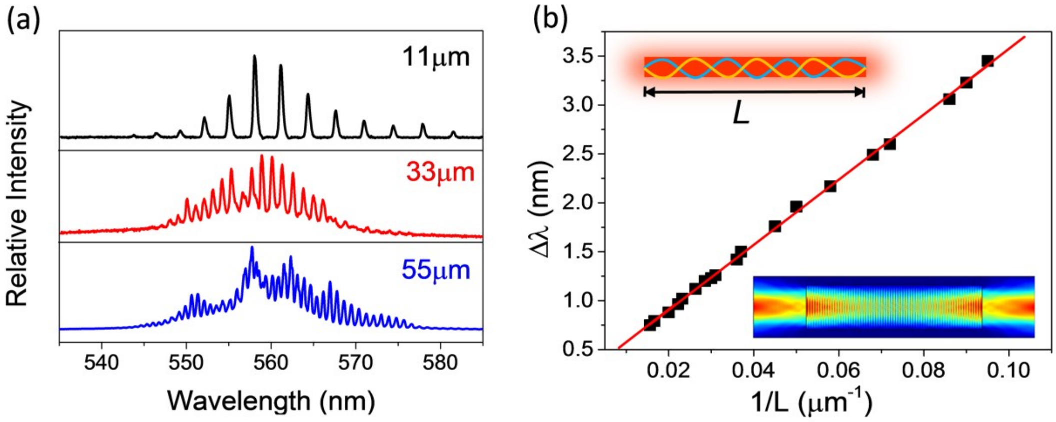

Fig. S15. (a) High resolution PL spectra of laser-emitted microribbons with length of l = 11, 33 and 55 μm, respectively. (b) The mode spacing $\Delta\lambda$ at λ 560 nm versus 1/L of microribbons, showing clearly a linear relationship. Top inset: illustrates a typical optical ray analysis within FP micro-cavity. Bottom inset: simulated 2D normalized electric field (λ= 560 nm, n = 1.80) in the cross section of microribbon (l = 12.5 μm and w = 3.3 μm).

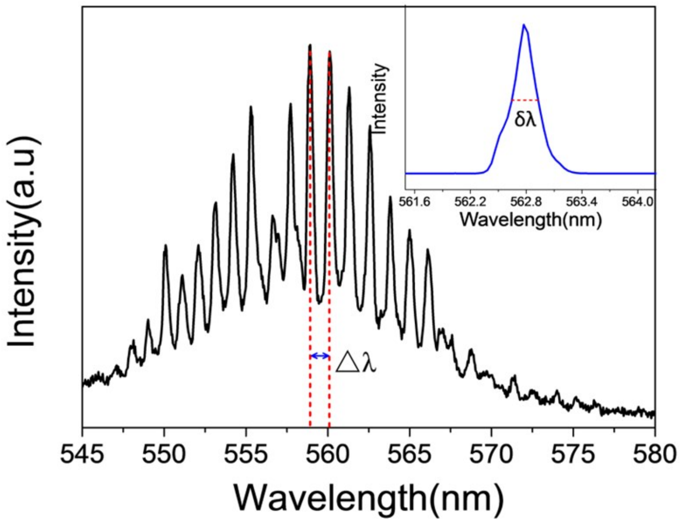

Fig. S16. The PL spectra (black curve) and peak-separation-fitting spectra (red curve) of 2D-MRs. Inset: The $\Delta\lambda L$ is the line-width of the peak around 562 nm.

The effect of MR size on cavity effect is further studied with a series of MRs with L = 11, 33 and 55 μm (Fig. S15a). Fig. S15a shows that the laser spectrum of the MR shows more and more patterns as the length of the MR is increased The spacing $\Delta\lambda$ between adjacent modes decreases at the same time as the MR length value increases, for example Δλ = 3.23, 1.23, 0.83 nm for L = 11, 33 and 55 μm, respectively. For the PL spectra of FP-type resonance, the mode spacing Δλ between two adjacent resonance peaks (Fig. S16) is given by $\Delta\lambda = \lambda^2/L[n- \lambda(dn/d\lambda)]$, Where λ is the wavelength of light, n is the phase refractive index, dn/ dλ is the dispersion relation and L is the round-trip distance within a cavity mode (a function of the length of MR: L = 2l).[7] A plot of the 1/L MR versus the mode spacing Δλ at 557 nm is shown in Fig. S15, and it is obvious that the relationship is linear. This not only confirms that the MR of SBF_2BTF operates as an FP mode resonator along its length rather than other dimensions of 2D-MR, but also further confirms that the built-in FP micro-cavity in the microribbon is well suited for the simulated electric field in the cross section of the MR (bottom inset of Fig. S15).

NMR spectra

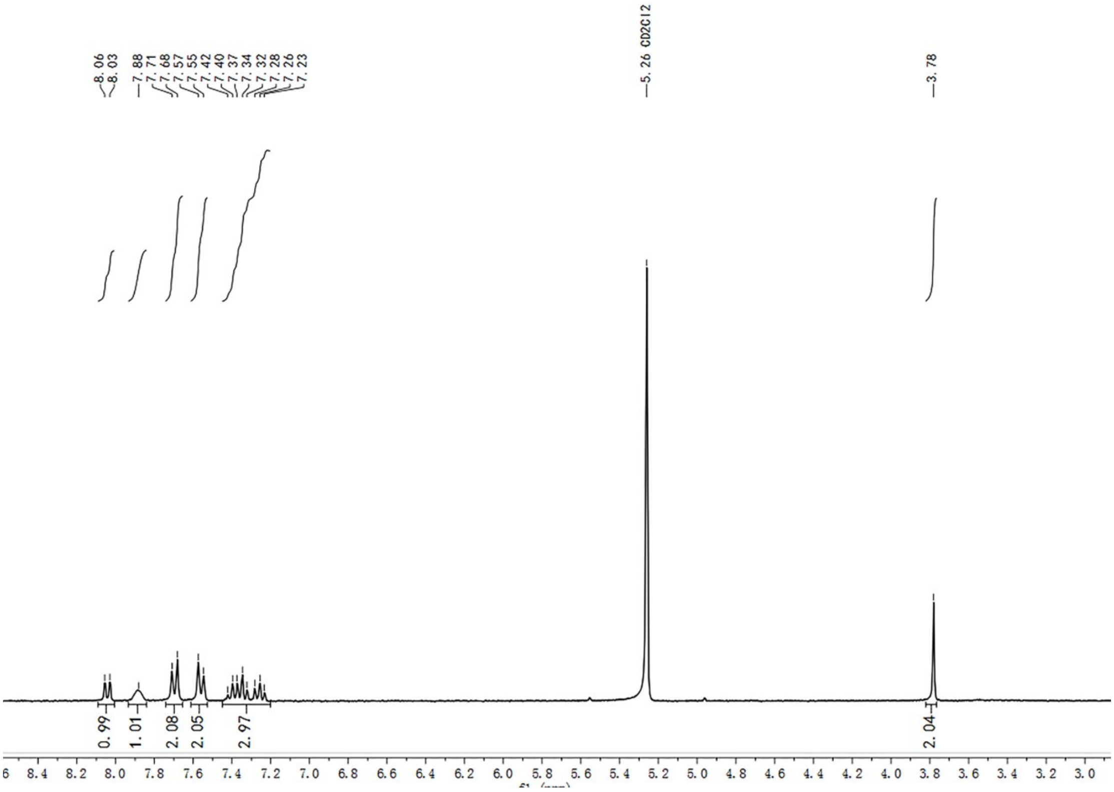

Fig. S17. ^{1}HNMR (400 MHz, CD_2Cl_2 300 K) of compound SBF_2BTF.

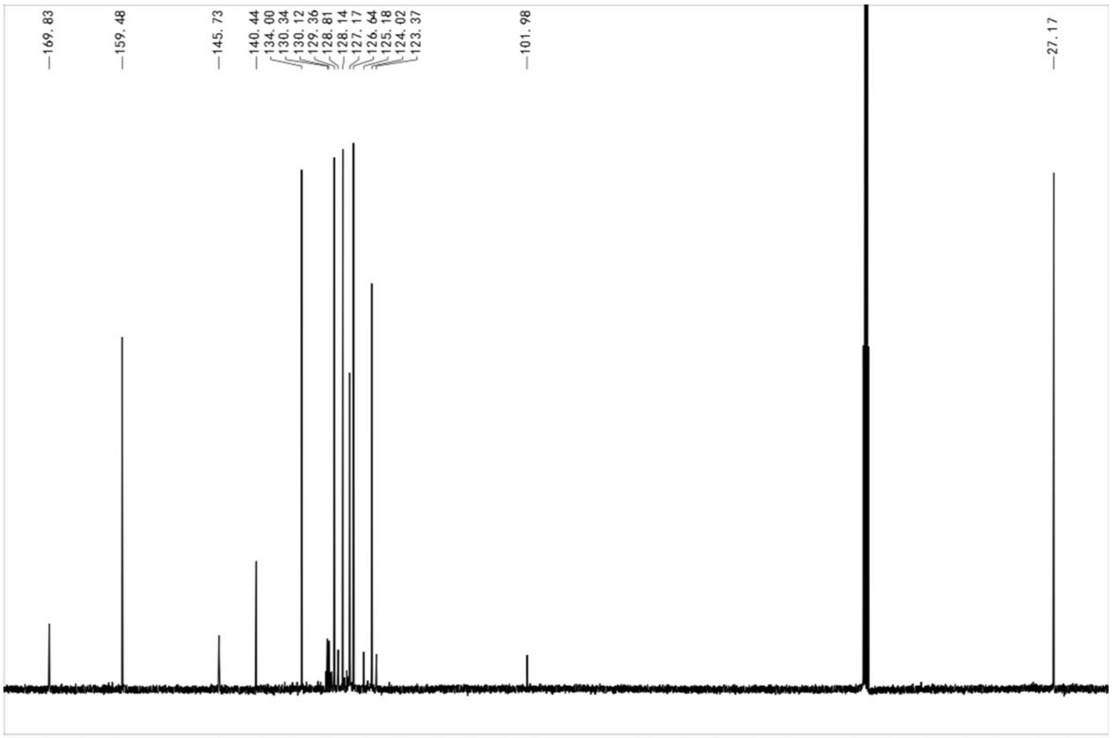

Fig. S18. ^{1}CNMR (151 MHz, $CDCl_3$ 300 K) of compound SBF_2BTF.

HR-MALDI

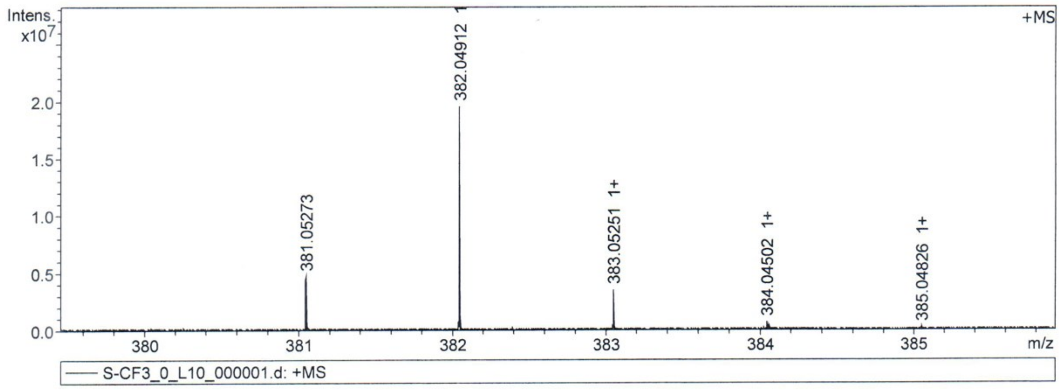

Fig. S19. HR-MALDI spectra of SBF_2BTF.

References

[1] a) G. J. Reddy, D. Latha, K. Pallavi, K. S. Rao, *Heterocycl.Commun.* **2003**, *9*, 453 b) G. Sivaprasad, R. Sridhar, P. T. Perumal, *J.Heterocycl.Chem.* **2006**, *43*, 389; c) K. Perumal, J. A. Garg, O. Blacque, R. Saiganesh, S. Kabilan, K. K. Balasubramanian, K. Venkatesan, *Chem. - Asian J.* **2012**, *7*, 2670.

[2] Z. J. Diwu, J. W. Lown, *J. Photochem. Photobiol. A-Chem.* 1992, 64, 273.

[3] Farkas, O.; Foresman,J. B.; Ortiz, J.V.; Cioslowski, J.; Fox, D. J. Gaussian, Inc.,Wallingford CT, **2010**.

[4] a) X. Gao, S. Bai, D. Fazzi, T. Niehaus, M. Barbatti, W. Thiel, *J. Chem. Theory Comput.***2017**, *13*, 515;b) http://bbs.keinsci.com/thread-9442-1-1.html, Mar , 2018.

[5] T. Lu, F. W. Chen, J. Comput. Chem. **2012**, *33*, 580-592

[6] Grabowski, Z. R.; Rotkiewicz, K.; Rettig, W. *Chem. Rev.* **2003,** *103* (10), 3899-4031.

[7] D. O'Carroll, I. Lieberwirth, G. Redmond, *Nat. Nanotechnol.* **2007**, *2*, 180.